Radiation Physics and Chemistry 145 (2018) 193–201

Contents lists available at ScienceDirect

Radiation Physics and Chemistry

journal homepage: www.elsevier.com/locate/radphyschem

A pulse-shape discrimination method for improving Gamma-ray spectrometry based on a new digital shaping filter

Zhang-jian Qin[a], Chuan Chen[a,*], Jun-song Luo[a], Xing-hong Xie[a], Liang-quan Ge[a], Qi-fan Wu[b]

[a] School of Information Science & Technology, Chengdu University of Technology, Chengdu, China
[b] Department of Engineering Physics, Tsinghua University, Beijing, China

ARTICLE INFO

Keywords:
Pulse-shape discrimination
Nuclear spectroscopy
Digital shaping filter
Mexican hat wavelet pulse

ABSTRACT

It is a usual practice for improving spectrum quality by the mean of designing a good shaping filter to improve signal-noise ratio in development of nuclear spectroscopy. Another method is proposed in the paper based on discriminating pulse-shape and discarding the bad pulse whose shape is distorted as a result of abnormal noise, unusual ballistic deficit or bad pulse pile-up. An Exponentially Decaying Pulse (EDP) generated in nuclear particle detectors can be transformed into a Mexican Hat Wavelet Pulse (MHWP) and the derivation process of the transform is given. After the transform is performed, the baseline drift is removed in the new MHWP. Moreover, the MHWP-shape can be discriminated with the three parameters: the time difference between the two minima of the MHWP, and the two ratios which are from the amplitude of the two minima respectively divided by the amplitude of the maximum in the MHWP. A new type of nuclear spectroscopy was implemented based on the new digital shaping filter and the Gamma-ray spectra were acquired with a variety of pulse-shape discrimination levels. It had manifested that the energy resolution and the peak-Compton ratio were both improved after the pulse-shape discrimination method was used.

1. Introduction

For more than two decades, advancements in Digital Pulse Processing (DPP) have made it one of the most utilized techniques in development of digital nuclear spectroscopy (Jordanov, 2016). A nuclear particle detector often generates an EDP which is caused by a nuclear particle. After the DPP is performed, the EDP can be transformed into another pulse shape, such as a trapezoidal pulse (Regadío et al., 2014), a bipolar trapezoidal pulse (Esmaeili-sani et al., 2012), a bipolar triangular pulse shaping (Esmaeili-sani et al., 2011), a Gaussian pulse shaping (Chen et al., 2009; Chen et al., 2008), among others. The DPP is usually called as pulse shaping filter and the signal-noise ratio is improved during the processing.

Though the signal-noise ratio is improved after the EDP being transformed into another pulse shape, perhaps the pulse amplitude is calculated incorrectly as a result of pulse's baseline drifting (Xu et al., 2015), or bad pulses being mixed in the good pulses. The shape of the bad pulse is often distorted as a result of abnormal noise, unusual ballistic deficit or bad pulse pile-up. A good DPP should remove the effects of baseline drifting, or discriminate the pulse-shape and discard the distorted pulse as well. In the neutron detector, the width of the pulse output from the preamplifier is not the same as when the pulse is caused by gamma and neutron particles (Zaitseva et al., 2013). Such particles can be discriminated and selected based on the pulse width parameter (Alharbi, 2016; Zhang et al., 2012; Asztalos et al., 2016; Balmer et al., 2015). Wavelet transform had been used to discriminate the pulses caused by a variety of nuclear particles (Yousefi et al., 2009). Inspired by this, based on the pulse-shape discrimination, discarding the distorted pulse, designing this type of Gamma-ray Spectrometry and acquiring the Gamma-ray Spectra, the Spectra quality perhaps would be improved.

2. Method

Fig. 1 shows the schematic diagram of the spectra acquisition chain. The EDP generated in a nuclear particle detector is amplified and converted into a digital one. Then the digital EDP is transformed into a MHWP with the MHWP shaping filter. The Multi-channel analyzer obtains the MHWP's height and constructs the spectra at last. Meanwhile the bad pulse-shape is discriminated and the distorted pulse is discarded.

The MHWP-shape can be represented easily with some parameters and the distorted pulse can be discriminated with the parameter values. As shown in Fig. 2, the amplitude of the maximum H in the MHWP is

* Corresponding author.
E-mail address: 17103738@qq.com (C. Chen).

http://dx.doi.org/10.1016/j.radphyschem.2017.10.023
Received 4 February 2017; Received in revised form 17 September 2017; Accepted 31 October 2017
Available online 02 November 2017
0969-806X/

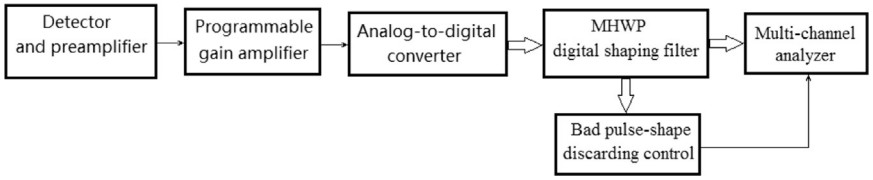

Fig. 1. Schematic diagram of the spectra acquisition chain.

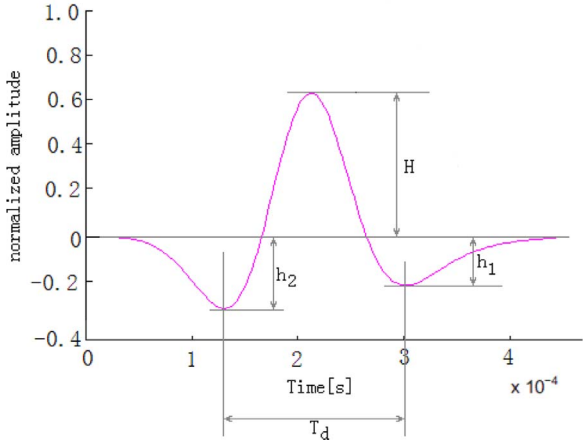

Fig. 2. MHWP-shape parameters represented with the $\frac{h_1}{H}$, $\frac{h_2}{H}$ and T_d.

the amplitude of the EDP caused by a nuclear particle. The MHWP-shape can be measured with the ratios $\frac{h_1}{H}$ and $\frac{h_2}{H}$, which are from the amplitudes of the two minima h_1 and h_2 respectively divided by the amplitude of the maximum H. The time difference T_d between the two minima can be also used to measure the MHWP-shape. If abnormal noise, unusual ballistic deficit or bad pulse pile-up appeared in the EDP, then the parameters $\frac{h_1}{H}$, $\frac{h_2}{H}$ and T_d would exceed the normal levels after the EDP was transformed into the MHWP.

Unlike Mexican hat wavelet transform applied in Gamma-ray Spectrometry as described in the literature (El Badri, et al., 2013), the MHWP shaping filter is a new digital shaping filter, which can transform an EDP into a MHWP. The impulse response of the filtering system should be deduced and a special-purpose digital logic circuit to process the filtering algorithm in real-time should also be designed.

3. Pulse shaping filter designing

It was assumed that when a particle is detected, the preamplifier stage will generate the following pulse:

$$x(t) = H\exp\left(-\frac{t}{\tau_0}\right)u(t) \tag{1}$$

where H is the pulse amplitude, τ_0 is the exponential decaying time constant, and $u(t)$ is the unit step function defined as follows:

$$u(t) = \begin{cases} 0, & t < 0 \\ 1, & t \geq 0 \end{cases} \tag{2}$$

The impulse response $h(t)$ is given by the following expression:

$$h(t) = \left[\frac{t^3}{s^4} - \frac{3t}{s^2} + \frac{1}{\tau_0}\left(1 - \frac{t^2}{s^2}\right)\right]\exp\left(-\frac{t^2}{2s^2}\right) \tag{3}$$

where s is the scale factor in the wavelet transform.

The transformation of an input signal x(t) into an output signal y(t) by a Linear Time-Invariant (LTI) system is mathematically expressed as the output signal as a convolution of the input signal and the impulse response of the system. The convolution is commonly written using the star (*) symbol. y(t) is given by the following expression:

$$y(t) = x(t)*h(t) = Hg\left(\frac{t}{s}\right) \tag{4}$$

where H is the pulse amplitude as shown in Eq. (1), s is the scale factor as shown in Eq. (3), and g(t) is a mother wavelet, namely defined as follows:

$$g(t) = (1 - t^2)\exp\left(-\frac{t^2}{2}\right) \tag{5}$$

The EDP, the impulse response and the output response of the system are depicted in Fig. 3.

Eq. (4) shows an important concept, which is deduced using the following formulas.

The property of the Fourier transform will be used in the following proof.

$$\text{if } f(t) \leftrightarrow F(\omega), \text{ then } \frac{d^n f(t)}{dt^n} \leftrightarrow (j\omega)^n F(\omega) \tag{6}$$

$$\text{if } f(t) \leftrightarrow F(\omega), \text{ then } f\left(\frac{t}{a}\right) \leftrightarrow aF(ja\omega)(a > 0) \tag{7}$$

The Fourier transform of a Gaussian signal will be used as well.

$$f(x) = \exp\left(-\frac{t^2}{2}\right) \leftrightarrow F(\omega) = \sqrt{2\pi}\exp\left(-\frac{\omega^2}{2}\right) \tag{8}$$

The wavelet basis function of g(t) convolution type is given by

$$g_s(t) = \frac{1}{s}g\left(\frac{t}{s}\right) \tag{9}$$

The derivative of g(t) is given by

$$\psi(t) = \frac{dg(t)}{dt} = (t^3 - 3t)\exp\left(-\frac{t^2}{2}\right) \tag{10}$$

The $\psi(t)$ in Eq. (10) is from the third derivative of $-\exp\left(-\frac{t^2}{2}\right)$. The Fourier transform of $\psi(t)$ is obtained with the Eqs. (6) and (8), as follows:

$$\hat{\psi}(\omega) = \sqrt{2\pi}j\omega^3\exp\left(-\frac{\omega^2}{2}\right) \tag{11}$$

The admissibility condition of a wavelet mother function is given by

$$C_\psi = \int_{-\infty}^{+\infty}\frac{|\hat{\psi}(\omega)|^2}{|\omega|}d\omega = 0 \tag{12}$$

$\psi(t)$ can be used as the wavelet mother function if $C_\psi < \infty$. The wavelet basis function of $\psi(t)$ convolution type is given by

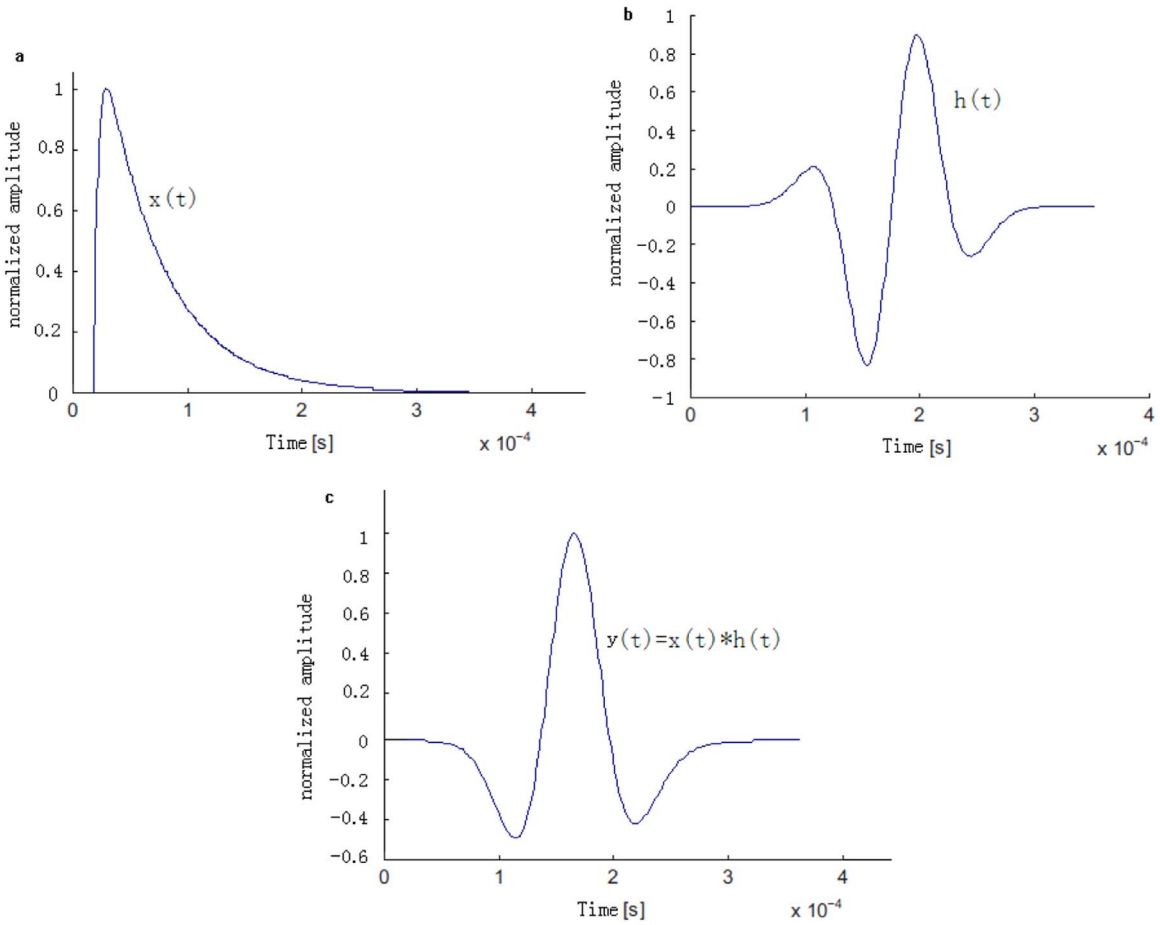

Fig. 3. Convolution of an EDP (a) with impulse response (b) and the output response of the system (c).

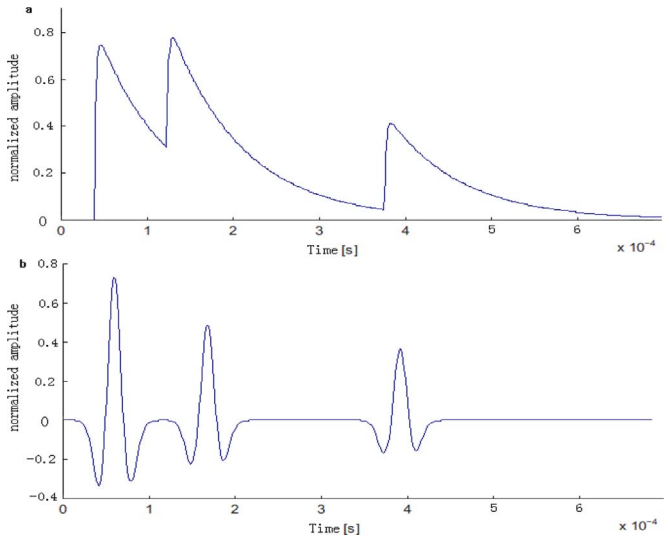

Fig. 4. EDPs with tail-pile-up (a) and output MHWPs without tail-pile-up (b).

$$\psi_s(t) = \frac{1}{s}\psi\left(\frac{t}{s}\right) \tag{13}$$

Using Eq. (13) as the wavelet basis function, the wavelet transform of Eq. (1) is given by:

$$\begin{aligned} & x(t)*\psi_s(t) \\ &= x(t)*s\frac{dg_s(t)}{dt} \\ &= \frac{dx(t)}{dt}*sg_s(t) \\ &= \left[-\frac{1}{\tau_0}x(t) + H\delta(t)\right]*sg_s(t) \end{aligned} \tag{14}$$

where $\delta(t)$ is the unit impulse, which is defined as:

$$\delta(t) = \begin{cases} 1, & t = 0 \\ 0, & t \neq 0 \end{cases} \tag{15}$$

According to Eq. (14), we can deduce the following:

$$\begin{aligned} & Hsg_s(t) = x(t)*\left[\psi_s(t) + \frac{s}{\tau_0}g_s(t)\right] \\ &= x(t)*\left[\frac{t^3}{s^4} - \frac{3t}{s^2} + \frac{1}{\tau_0}\left(1 - \frac{t^2}{s^2}\right)\right]\exp\left(-\frac{t^2}{2s^2}\right) \end{aligned} \tag{16}$$

According to Eqs. (5) and (9), Eq. (17) can be deduced:

$$Hg\left(\frac{t}{s}\right) = Hsg_s(t) \tag{17}$$

Eqs. (16) and (17) have given the proof of the Eq. (4). Because the impulse response of the filtering system $h(t)$ as described in Eq. (3) is a second-order smooth function, the convolution of a linear baseline with $h(t)$ is identically equal to zero. The following is the derivation process.

A linear baseline is given by

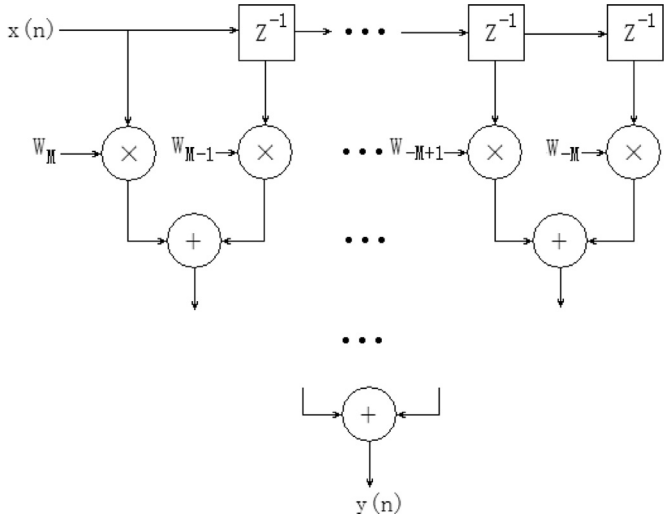

Fig. 5. The special-purpose DLC for processing the digital filtering in real-time.

$$b(t) = kt + c \tag{18}$$

Convolution of b(t) with h(t) is given by

$$\begin{aligned} b(t)^{*}h(t) &= k\int_{-\infty}^{+\infty}\left[\frac{(t-\tau)\tau^3}{s^4} - \frac{3(t-\tau)\tau}{s^2}\right. \\ &\quad \left. + \frac{1}{\tau_0}\left(t-\tau-\frac{(t-\tau)\tau^2}{s^2}\right)\right]\exp\left(-\frac{\tau^2}{2s^2}\right)d\tau \\ &\quad + c\int_{-\infty}^{+\infty}\left[\frac{\tau^3}{s^4} - \frac{3\tau}{s^2} + \frac{1}{\tau_0}\left(1-\frac{\tau^2}{s^2}\right)\right]\exp\left(-\frac{\tau^2}{2s^2}\right)d\tau \\ &= -\frac{k}{s^4}\int_{-\infty}^{+\infty}\tau^4\exp\left(-\frac{\tau^2}{2s^2}\right)d\tau + \frac{3k}{s^2}\int_{-\infty}^{+\infty}\tau^2\exp\left(-\frac{\tau^2}{2s^2}\right)d\tau \\ &\quad + \frac{kt+c}{\tau_0}\int_{-\infty}^{+\infty}\exp\left(-\frac{\tau^2}{2s^2}\right)d\tau \\ &\quad - \frac{kt+c}{s^2\tau_0}\int_{-\infty}^{+\infty}\tau^2\exp\left(-\frac{\tau^2}{2s^2}\right)d\tau \\ &= -3\sqrt{2\pi}ks + 3\sqrt{2\pi}ks + \frac{kt+c}{\tau_0}\sqrt{2\pi}s - \frac{kt+c}{\tau_0}\sqrt{2\pi}s \\ &= 0 \end{aligned} \tag{19}$$

The integral computation in formula (19) must apply the conclusions of Eqs. (20)–(22):

$$\int_{-\infty}^{+\infty}\exp\left(-\frac{t^2}{2s^2}\right)dt = s\sqrt{2\pi} \tag{20}$$

$$\int_{-\infty}^{+\infty}t^{2n}\exp\left(-\frac{t^2}{2s^2}\right)dt = 1\bullet 3\bullet \ldots \bullet(2n-1)\bullet s^{2n+1}\sqrt{2\pi},\ n = 1, 2, \ldots \tag{21}$$

$$\int_{-\infty}^{+\infty}t^{2n-1}\exp\left(-\frac{t^2}{2s^2}\right)dt = 0,\ n = 1, 2, \ldots \tag{22}$$

According to Eq. (19), a linear baseline overlapped on the EDP can be removed after the pulse is transformed into a MHWP.

The width of the MHWP is determined with the value of the scale factor s as described in Eq. (3). If the value of s is suitable, the pile-up will be eliminated in the MHWP even though a pile-up exists in the EDP before performing the transform. As shown in Fig. 4(a), there is an obvious pile-up in the EDPs. After the pulses are transformed into the MHWPs, the pile-up is completely eliminated in Fig. 4(b).

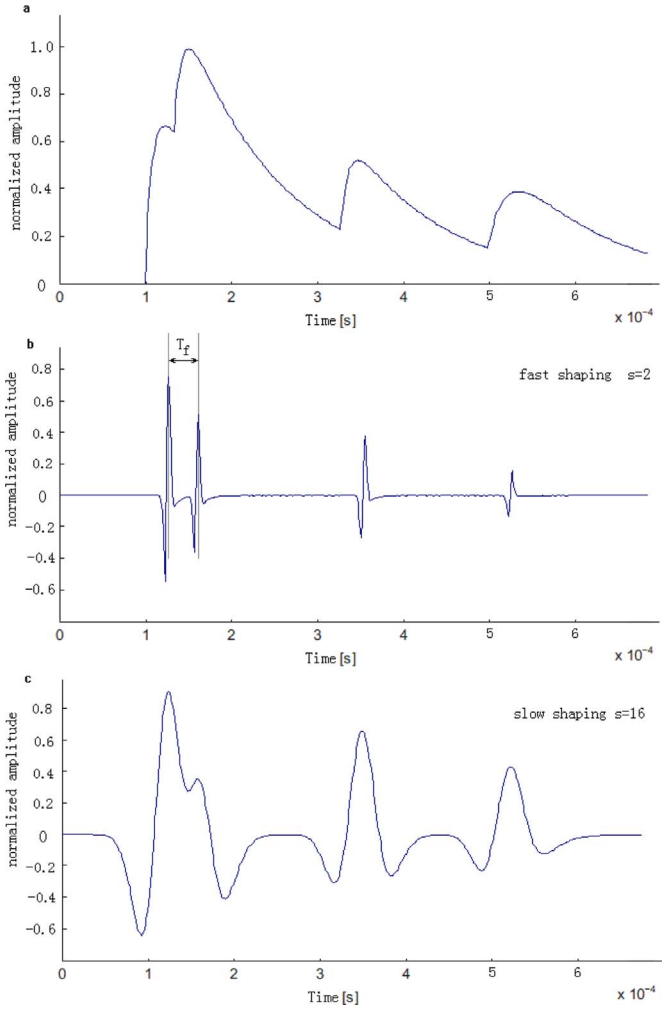

Fig. 6. Pulse selected by parameter T_f(b).

Obviously, the Eq. (3) meets the following condition:

$$\lim_{|t|\to\infty} h(t) = 0 \tag{23}$$

Therefore, in the discrete domain, we have:

$$h(n) = \begin{cases} w_n = \left[\frac{n^3}{s^4} - \frac{3n}{s^2} + \frac{1}{\tau_0}\left(1-\frac{n^2}{s^2}\right)\right]\exp\left(-\frac{n^2}{2s^2}\right),\ |n| = 0, 1, 2, \ldots\ldots, M \\ 0,\ |n| > M \end{cases} \tag{24}$$

where M is a sufficient positive integer, and s is the scale factor in the wavelet transform.

In the discrete domain, Eq. (4) can be rewritten as follows:

$$y(n) = \sum_{i=-M}^{M} x(n-i)\bullet w_i \tag{25}$$

If a linear baseline is considered, x(n) is given as Eq. (26):

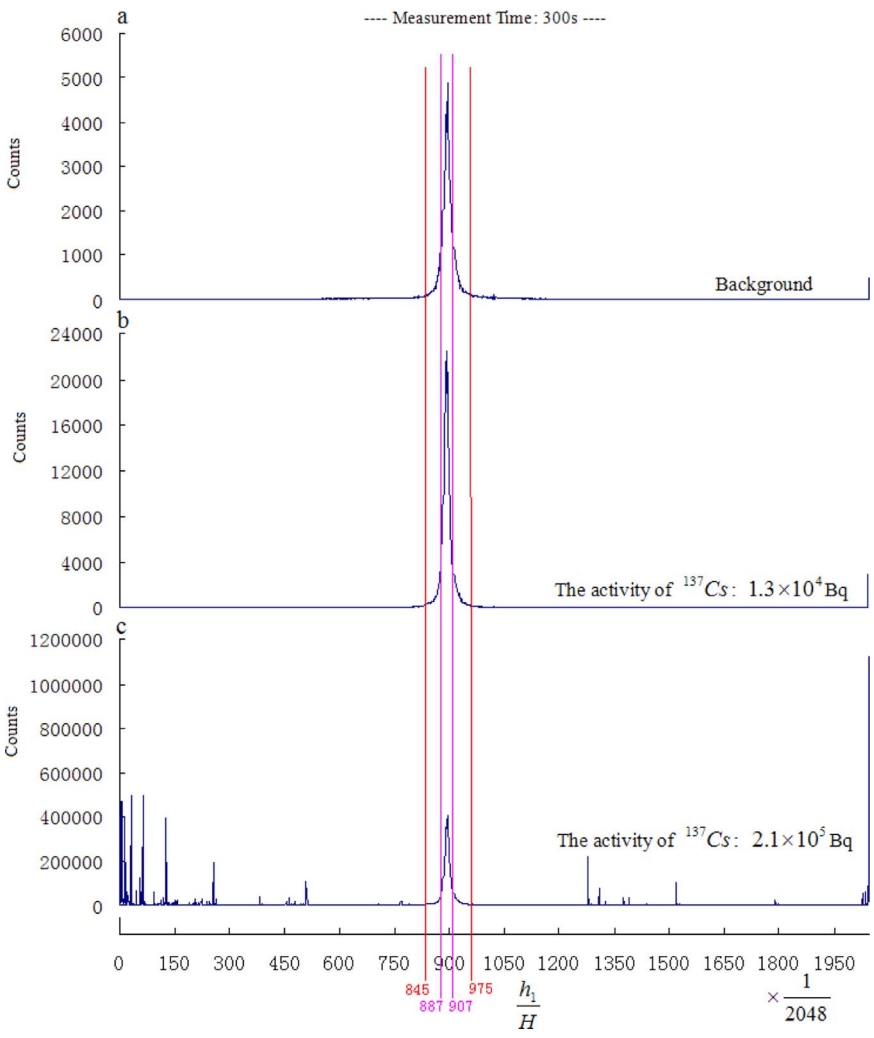

Fig. 7. MHWP-shape parameter $\frac{h_1}{H}$ spectra with a variety of count rates.

$$x(n)=\begin{cases} kn+c, & n=\ldots,-2,-1, \\ \mathrm{X_n}=kn+c+\mathrm{H}\exp\left(-\frac{n}{\tau_0}\right), & \mathrm{n}=0,1,\ldots,3\mathrm{N}-1 \\ \mathrm{kn}+\mathrm{c}, & \mathrm{n}=3\mathrm{N},3\mathrm{N}+1,\ldots \end{cases} \tag{26}$$

Where k is a coefficient, c is a constant, H is the pulse amplitude, τ_0 is exponential decaying time constant, and N is a positive integer.

If X_n(n = 0,1,…,3N-1) in Eq. (26) is the EDP sampling point sequence, then τ_0 can be obtained using Eq. (27) (Z. J. Qin et al., 2007), as follows:

$$\tau_0=\frac{N}{\ln\frac{\sum_{i=N}^{2N-1}X_i-\sum_{i=0}^{N-1}X_i}{\sum_{i=2N}^{3N-1}X_i-\sum_{i=N}^{2N-1}X_i}} \tag{27}$$

The real-time computation in Eq. (25) can be achieved with the Digital Logic Circuit (DLC) in Fig. 5. In total, 187 multipliers and 186 adders are adopted in the prototype in this study, and the DLC is implemented by a Field-Programmable Gate Array (FPGA) chip. The convolution calculation of a sample point can be processed in a sampling clock cycle by the DLC, which is processed in real-time absolutely. Z^{-1} in Fig. 5 means one clock cycle delay of the input signal, which can be implemented by a D-Trigger digital logic unit.

4. Pulse-shape discrimination method

As we can know, the value of the scale factor s determines the width of the MHWP. If the value of s is set too small, then the width of the MHWP will become very narrow and the pile-up will not exist, but the amplitude of the MHWP will be calculated inaccurately because the number of sample points is too few when Eq. (25) is used to transform an EDP into a MHWP in the discrete domain. If the value of s is set too high, though the amplitude of the MHWP is calculated accurately, perhaps the pile-up will not be eliminated because the width of the MHWP is too wide. To deal with the contradiction, both fast shaping filter and slow shaping filter are used. The fast shaping filter counts the pulse number and the slow shaping filter calculates the pulse amplitude. The slow MHWPs are shown in Fig. 6(c), which are shaped by slow shaping filter where s = 16. The fast MHWPs are shown in Fig. 6(b), which are shaped by fast shaping filter where s = 2. T_f in Fig. 6(b) is the time difference between two adjacent pulses. If the value of T_f is too small, then the pile-up will still exist in the slow MHWPs, as shown in Fig. 6(c). Under this circumstance, the amplitude of the two adjacent pulses cannot be obtained correctly, and therefore, the two adjacent pulses should be discarded.

Besides the fast and slow shaping method, the pulse-shape

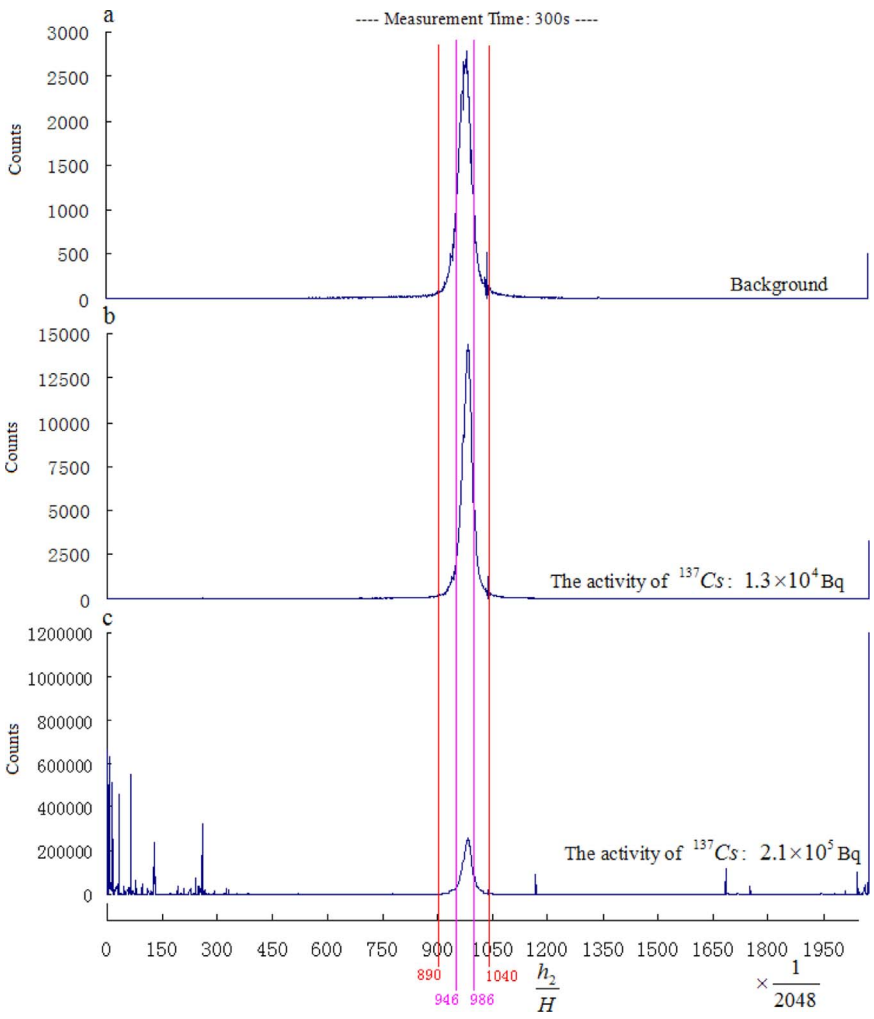

Fig. 8. MHWP-shape parameter $\frac{h_2}{H}$ spectra with a variety of count rates.

discrimination method can be used for improving the spectrum quality. As shown in Fig. 2, $\frac{h_1}{H}$, $\frac{h_2}{H}$ and T_d are all pulse-shape parameters. Even one of the pulse-shape parameter values in a MHWP exceeds the normal level, we can judge the MHWP is a bad pulse whose shape is distorted perhaps as a result of abnormal noise, unusual ballistic deficit or bad pulse pile-up, and therefore, the pulse should be discarded. As shown in Fig. 7, Figs. 8 and 9, $\frac{h_1}{H}$, $\frac{h_2}{H}$ and T_d spectra with a variety of count rates were acquired, and the spectra respectively distributed as a Gaussian. Especially, the bad pulses increased dramatically because the pulse pile-up occurred frequently when the count rate was too high. The phenomenon had been shown in Fig. 7(c), Figs. 8(c) and 9(c). Pulses can be selected with the parameters $\frac{h_1}{H}$, $\frac{h_2}{H}$ and T_d, and the bad pulses can be easily discarded. Based on the pulse-shape discrimination method, the gamma-ray spectrum quality would be improved.

5. Experimental results

Fig. 10 shows a prototype of a nuclear spectrometer based on the new digital shaping filter and the pulse-shape discrimination method. A high-performance analog-to-digital converter (ADC) chip is used; the chip has 14-bit resolution, and a 125 Msps sample rate. An FPGA chip comprising 252 $18bit \times 18bit$ multipliers is used to process MHWP shaping filtering in real-time.

Energy resolution and peak-Compton ratio are usually used to evaluate the gamma spectra. The energy resolution is defined as the ratio of the full width at half maximum (FWHM) energy to the Gaussian peak energy. A $\Phi 75mm \times 75mm$ NaI(Tl) scintillator is used in the experiment, whose energy resolution nominal value is < 8.0%@662 keV (^{137}Cs), which is measured by the manufacturer. Peak-Compton is defined as the ratio of the Gaussian peak net height to the Compton background.

The experimental purpose is to verify whether or not the spectrum quality is improved with a variety of pulse-shape discrimination levels. Three different levels of pulse-shape discrimination parameter groups are as follows: (1) no pulse-shape discrimination; (2) $56 \le T_d \le 59$, $845 \le \frac{h_1}{H} \le 975$, $890 \le \frac{h_2}{H} \le 1040$; and (3) $56 \le T_d \le 59$, $887 \le \frac{h_1}{H} \le 907$, $946 \le \frac{h_2}{H} \le 986$. The spectra were acquired with a variety of count rates represented by three samples with the different activity levels, as follows: (1) natural background; (2) ^{137}Cs with the activity of 1.3×10^4 Bq; and (3) ^{137}Cs with the activity of 2.1×10^5 Bq. As shown in Figs. 11–13, both the energy resolution and peak-Compton ratio in the spectra were improved more and more when the value range of the pulse-shape discrimination parameters were set smaller and smaller. Especially, noises increased dramatically in the spectrum as shown in Fig. 13(a) when the count rate was too high and the pulse pile-up occurred frequently. After pulse-shape discrimination method was used, the noises reduced sharply in the spectra as shown in Fig. 13(b) and (c). The experimental results showed ten percent or more

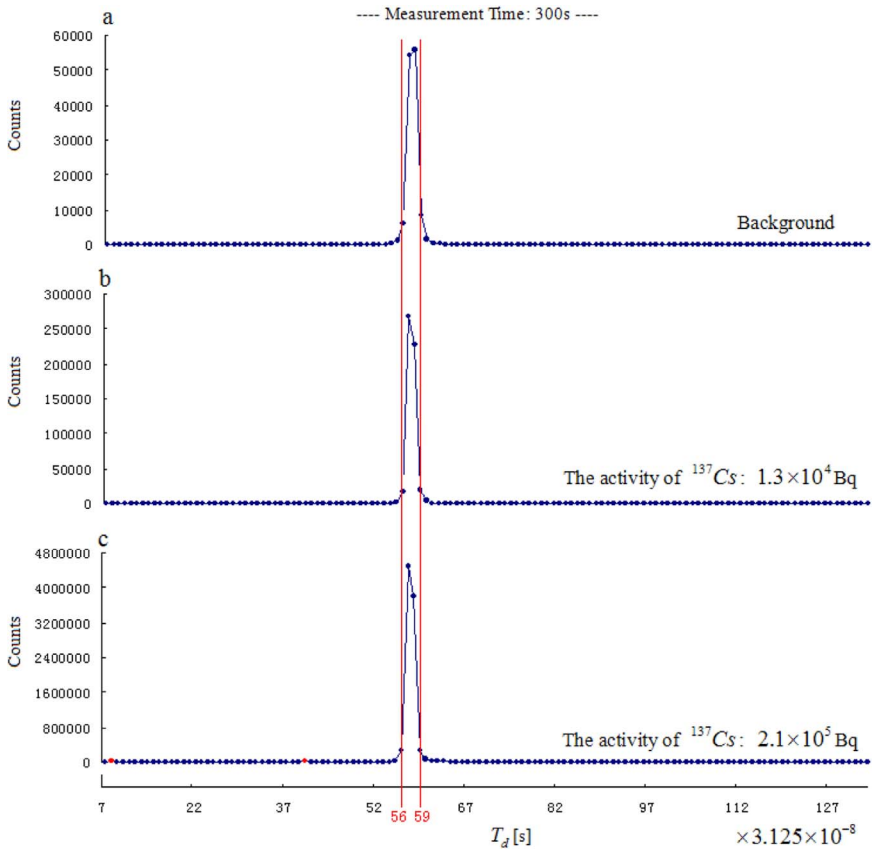

Fig. 9. MHWP-shape parameter T_d spectra with a variety of count rates.

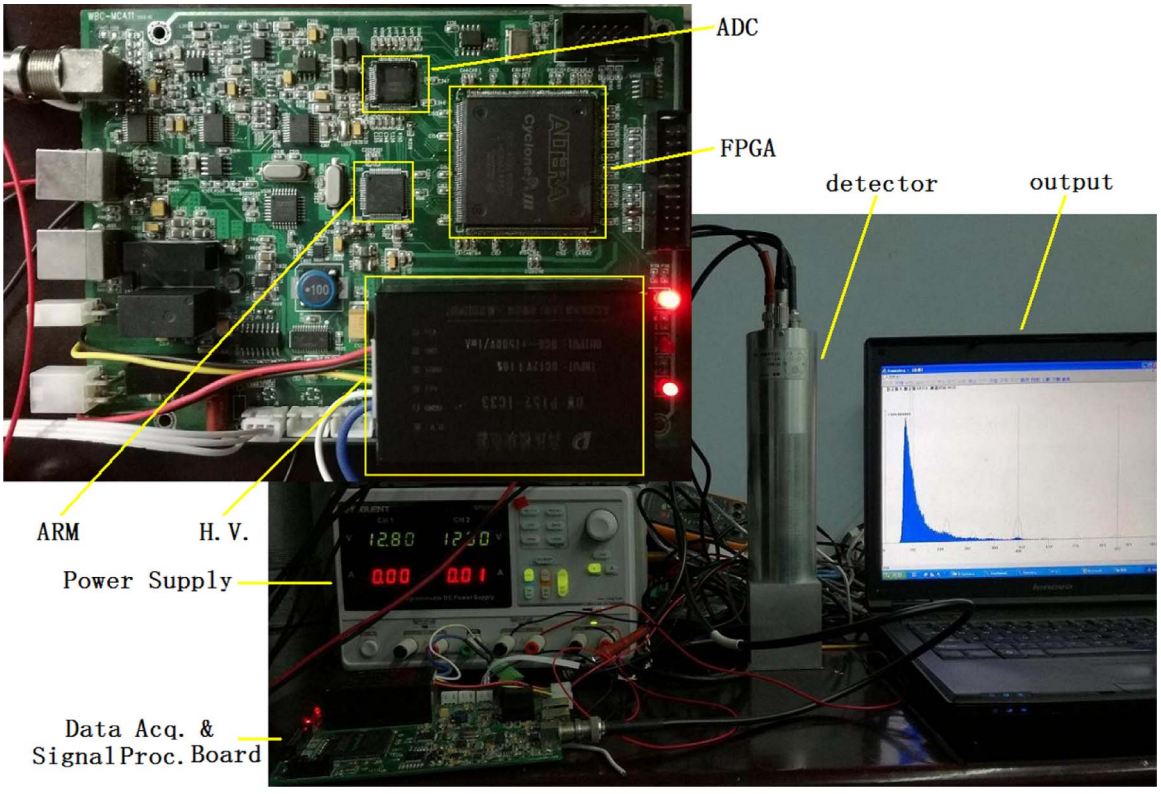

Fig. 10. Prototype of the nuclear spectrometer based on a MHWP shaping filter.

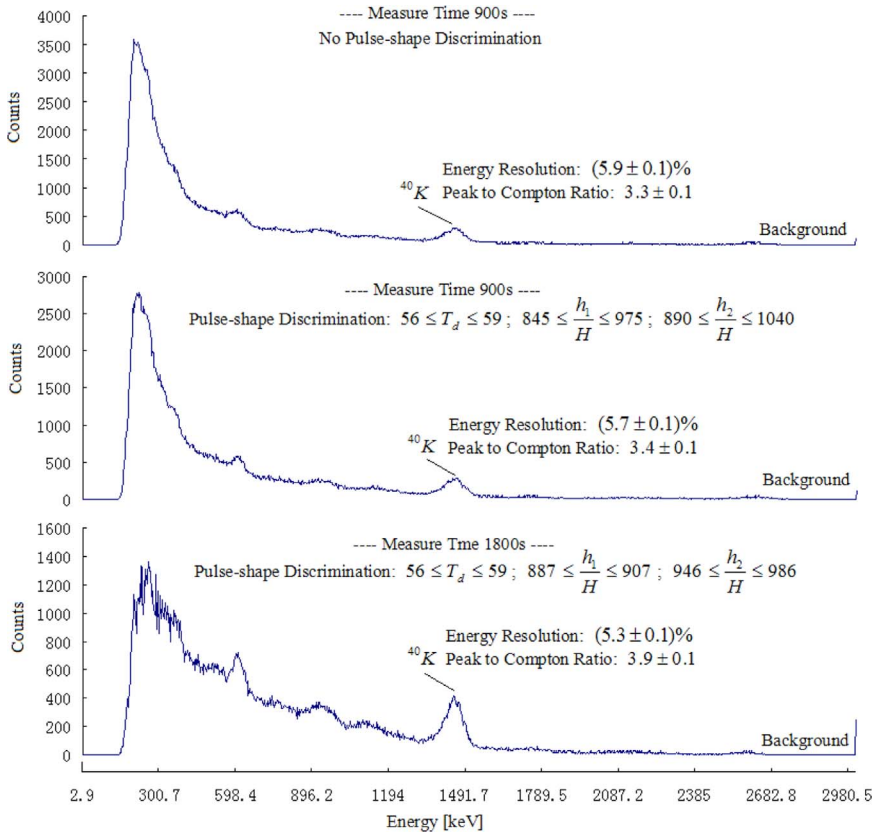

Fig. 11. Gamma energy spectra of natural background with a variety of pulse-shape discrimination levels.

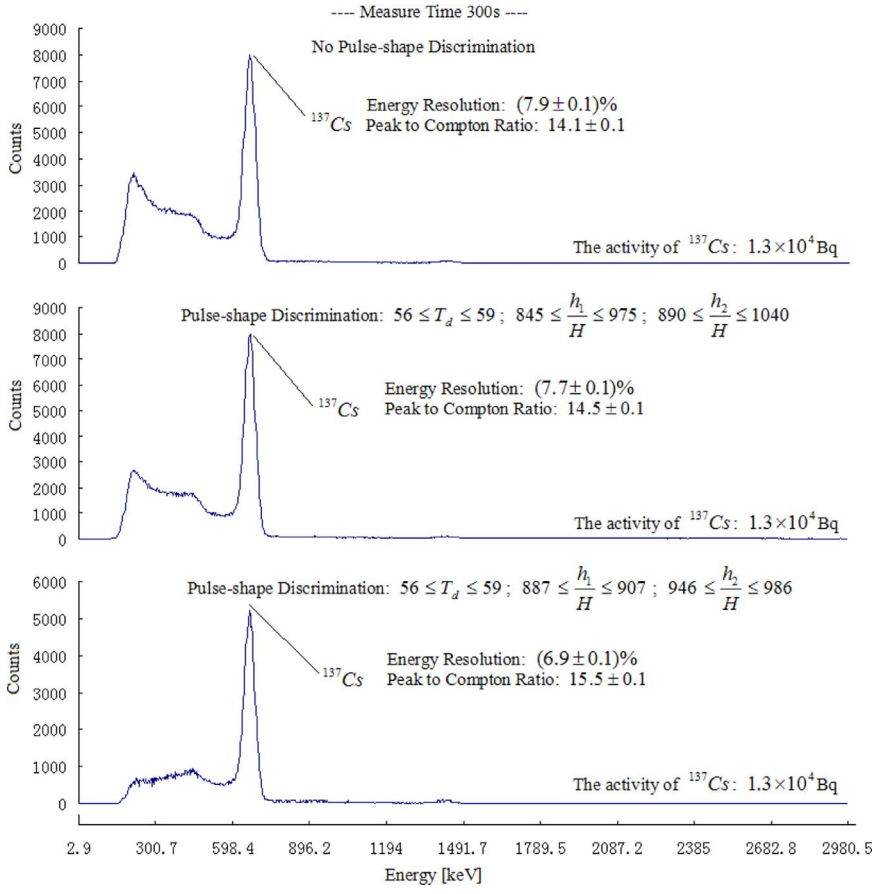

Fig. 12. Gamma energy spectra of 1.3×10^4 Bq ^{137}Cs with a variety of pulse-shape discrimination levels.

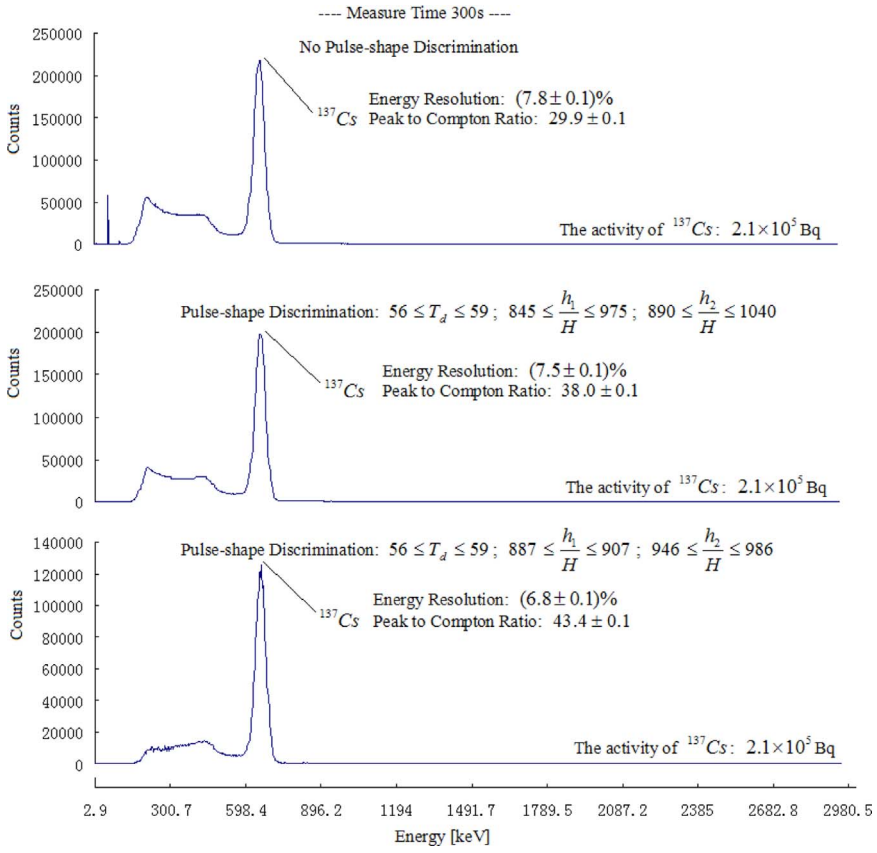

Fig. 13. Gamma energy spectra of 2.1×10^5 Bq ^{137}Cs with a variety of pulse-shape discrimination levels.

improvement in the energy resolution when the spectra were acquired with the strict pulse-shape discrimination.

6. Conclusions

After transforming an EDP into a MHWP, the amplitude of the EDP can be measured with the maximum of the MHWP. The MHWP-shape can be measured with the parameters: the time difference between the two minima of the MHWP, and the two ratios which are from the amplitude of the two minima respectively divided by the amplitude of the maximum in the MHWP.

The transform from an EDP into a MHWP depends on a new digital shaping filter. The impulse response function of the new digital shaping filter was deduced by using wavelet analysis technology. With hundreds of adders and multipliers working in parallel, the DPP can be processed in real-time.

A new nuclear spectrometer prototype was implemented and the pulse-shape discrimination method was used. Both the energy resolution and peak-Compton ratio were improved when the spectra were acquired with the pulse-shape discrimination.

Acknowledgments

This project was supported by the National Key R&D Program of China (Grant No. 2017YFC0602100).

References

Alharbi, T., 2016. Nucl. Instrum. Methods Phys. Res. A 806, 240.
Asztalos, Stephen J., et al., 2016. Nucl. Instrum. Methods Phys. Res. A 806, 132.
Balmer, Matthew J.I., et al., 2015. Nucl. Instrum. Methods Phys. Res. A 788, 146.
Chen, S.G., et al., 2008. Acta Phys. Sin. 57, 2882.
Chen, S.G., et al., 2009. Acta Phys. Sin. 58, 57.
El Badri, L., et al., 2013, Proceedings of the 3rd International Conference on Advancements in Nuclear Instrumentation, Measurement Methods and their Applications (ANIMMA), Marseille, France.
Esmaeili-sani, Vahid, et al., 2011. Nucl. Instrum. Methods Phys. Res. A 665, 11.
Esmaeili-sani, Vahid, et al., 2012. Nucl. Instrum. Methods Phys. Res. A 694, 113.
Jordanov, Valentin T., 2016. Nucl. Instrum. Methods Phys. Res. A 805, 63.
Z.J. Qin, et al., 2007, Journal of Cheng Du Univ. of Tech.(Scie. & Tech. Edit.)34, 643.
Regadío, Alberto, et al., 2014. Nucl. Instrum. Methods Phys. Res. A 735, 297.
Xu, H., et al., 2015. Nucl. Sci. Tech. 26, 050402.
Yousefi, S., et al., 2009. Nucl. Instrum. Methods Phys. Res. A 598, 551.
Zaitseva, N., et al., 2013. Nucl. Instrum. Methods Phys. Res. A 729, 747.
Zhang, X., et al., 2012. Nucl. Instrum. Methods Phys. Res. A 687, 7.